Crystal Structure of the Peroxisome Proliferator-Activated Receptor γ (PPARγ) Ligand Binding Domain Complexed with a Novel Partial Agonist: A New Region of the Hydrophobic Pocket Could Be Exploited for Drug Design

Roberta Montanari,[†] Fulvio Saccoccia,[†] Elena Scotti,[‡] Maurizio Crestani,[‡] Cristina Godio,[‡] Federica Gilardi,[‡] Fulvio Loiodice,[§] Giuseppe Fracchiolla,[§] Antonio Laghezza,[§] Paolo Tortorella,[§] Antonio Lavecchia,[∥] Ettore Novellino,[∥] Fernando Mazza,[†,⊥] Massimiliano Aschi,[⊥] and Giorgio Pochetti*[,†]

Consiglio Nazionale delle Ricerche, Roma 00016, Italy, Università degli Studi di Milano, Milano 20133, Italy, Università degli Studi di Bari, Bari 70125, Italy, Università degli Studi di Napoli "Federico II", Napoli 80131, Italy, and Università di L'Aquila, L'Aquila 67010, Italy

Received June 17, 2008

The peroxisome proliferator-activated receptors (PPARs) are ligand-dependent transcription factors regulating glucose and lipid metabolism. The search for new PPAR ligands with reduced adverse effects with respect to the marketed antidiabetic agents thiazolidinediones (TZDs) and the dual-agonists glitazars is highly desired. We report the crystal structure and activity of the two enantiomeric forms of a clofibric acid analogue, respectively complexed with the ligand-binding domain (LBD) of PPARγ, and provide an explanation on a molecular basis for their different potency and efficacy against PPARγ. The more potent *S*-enantiomer is a dual PPARα/PPARγ agonist which presents a partial agonism profile against PPARγ. Docking of the *S*-enantiomer in the PPARα-LBD has been performed to explain its different subtype pharmacological profile. The hypothesis that partial agonists show differential stabilization of helix 3, when compared to full agonists, is also discussed. Moreover, the structure of the complex with the *S*-enantiomer reveals a new region of the PPARγ-LBD never sampled before by other ligands.

Introduction

PPARs[a] belong to the nuclear receptors superfamily,[1,2] and they are transcription factors activated by specific ligands, which are usually lipophilic small molecules.[3] Binding of these ligands results in conformational changes of the receptors that facilitate their interaction with coactivator proteins in the nucleus.[2,4,5] The resulting protein complexes activate the transcription of specific target genes, resulting in the induction of intracellular signalling cascades that mediate the physiological effects of the ligands.[6,7]

So far, three PPAR subtypes have been described in mammals: PPARα, PPARγ, and PPARβ/δ. All of these are targets for treatment of the metabolic syndrome, a cluster of risk factors for cardiovascular disease and diabetes including obesity, atherogenic dyslipidemia, hypertension, insulin resistance, and elevated fasting blood glucose.[2] The fibrate class of lipid-lowering drugs (e.g., fenofibrate and gemfibrozil) are PPARα ligands.[8−10] The marketed TZD class of antidiabetic agents (rosiglitazone and pioglitazone) activates PPARγ.[11,12] They enhance insulin sensitivity in target tissues and lower glucose and fatty acid levels in type 2 diabetic patients. However, despite their proven benefits, these drugs have been plagued by certain adverse effects such as weight gain, higher rate of bone fractures, fluid accumulation, and pulmonary edema, leading to increased frequency of congestive heart failure.[13−15] A new class of dual agonists, glitazars, have elicited high hopes and deep disappointment as potential new drugs. Also known as PPARα/PPARγ dual agonists, glitazars are designed to treat both insulin resistance and key aspects of dyslipidemia that contribute to the high risk of cardiovascular diseases in diabetics. The two lead compounds in this class are muraglitazar and tesaglitazar, but both drugs were discontinued because of important side effects.[14,15] One of the key challenges for the development of a dual agonist is identifying the optimal receptor subtype selectivity ratio. The intrinsic potencies at each receptor subtype will ultimately determine the overall efficacy with respect to metabolic effects and minimized side effects. All failed PPAR agonists to date are apparently pure PPARγ or PPARγ-preferential dual agonists. Consequently, most safety issues that led to development discontinuations are rather associated with overactivation of PPARγ than with action on the α subtype. New drugs, which act as partial agonists of PPARγ, have been developed with the goal of retaining the beneficial effects while diminishing the adverse effects. Metaglidasen (see Figure 1), a PPARγ partial agonist, is the most advanced insulin sensitizer that is currently in phase III clinical trials. The results of phase II clinical trials showed that metaglidasen, a prodrug ester that is rapidly and completely modified in vivo to its mature circulating free acid form, significantly improved metabolic parameters without the side effects of fluid retention/edema or weight gain.[14] Recently, we reported the synthesis and activity of some chiral clofibric acid analogues[16] whose structures are

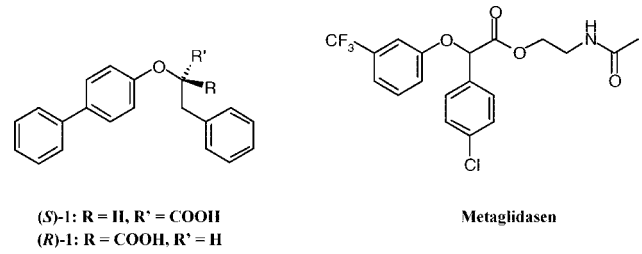

(*S*)-**1**: R = H, R' = COOH
(*R*)-**1**: R = COOH, R' = H

Metaglidasen

Figure 1. Chemical structures of (*S*)-**1**, (*R*)-**1**, and metaglidasen.

* To whom correspondence should be addressed. Phone: 0039.06.90672627. Fax: 0039.06.90672630. E-mail: giorgio.pochetti@ic.cnr.it.
[†] Consiglio Nazionale delle Ricerche.
[‡] Università degli Studi di Milano.
[§] Università degli Studi di Bari.
[∥] Università degli Studi di Napoli "Federico II".
[⊥] Università di L'Aquila.

[a] Abbreviations: PPAR, peroxisome proliferator-activated receptor; TZD, thiazolidinediones; LBD, ligand-binding domain; PDB, Brookhaven Protein Data Bank; MD, molecular dynamics; RMSF, root mean square fluctuation.

10.1021/jm800733h CCC: $40.75
Published on Web 11/18/2008

Scheme 1. Synthesis of (*S*)-**1**[a]

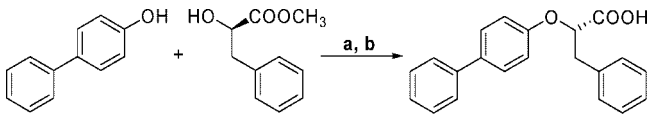

[a] (a) PPh_3-PS, DIAD, toluene; (b) THF, 1 N NaOH (1:1).

related to that of the active metabolite of metaglidasen. These compounds show dual activity toward PPARα and PPARγ with the stereochemistry playing a crucial role in the receptor activation. In the search for a well balanced dual agonist, we focused our attention on full agonist (*S*)-**1** (Figure 1) displaying a selectivity ratio equal to 1. A more in-depth investigation of PPARα/PPARγ agonist activity of this ligand and its enantiomer revealed that the former has a lower efficacy on PPARγ compared to that previously reported[16] and is about 10 times more potent than the latter. On the other hand, the *R*-enantiomer is completely devoid of activity on PPARα. Here, we report the X-ray structures of the PPARγ-LBD in the complex with (*S*)-**1** and (*R*)-**1**, respectively, and compare their structures, providing a molecular explanation for their different potency against PPARγ. Moreover, we compare the structure of the more potent *S*-enantiomer with that of the same ligand docked in the hydrophobic pocket of PPARα and provide an explanation at the molecular level for its different behavior as full and partial agonist of PPARα and PPARγ, respectively. Noteworthy, we also characterize a new region of the PPARγ internal hydrophobic pocket never sampled before by other PPARγ agonists that could be exploited in the design of new PPAR ligands.

Results and Discussion

Chemistry. The two enantiomers (*S*)-**1** and (*R*)-**1** were obtained as previously reported[16] by a two-step procedure including the condensation of 4-phenylphenol with the optically active methyl phenyllactates under Mitsunobu conditions followed from alkaline hydrolysis (in Scheme 1 the synthesis of (*S*)-**1** is depicted). However, the employment of triphenylphosphine supported on cross-linked styrene/divinylbenzene copolymer resin (PPh_3-PS) allowed us to simplify the workup of the first reaction and to improve the overall yield from 39% to 77−81%, leaving unchanged the enantiomeric excess of ≥98%.

Transcriptional Activation of PPARα and γ Subtypes by (*S*)-1 and (*R*)-1. In previous studies we had shown that new enantiomeric compounds were active toward both the PPARα and γ subtypes.[16] To gain more insight on the activity of one of these ligands displaying a selectivity ratio equal to 1, we first determined the effect of its enantiomeric forms, (*S*)-**1** and (*R*)-**1**, on the transcriptional activity of a panel of nuclear receptors. As shown in Figure 2A, (*S*)-**1** activates both PPARα and PPARγ but does not affect the transcriptional activity of the other tested nuclear receptors. Conversely, (*R*)-**1** activates only PPARγ. We next compared the potency and efficacy of the two enantiomers to those of the known PPARα and γ agonist, Wy 14,643 and rosiglitazone, respectively. The concentration−response curves obtained from cell-based assays indicate that (*S*)-**1** is a more potent PPARα agonist than Wy 14,643, here used as the reference (Figure 2B). The EC_{50} of (*S*)-**1** is about 1 order of magnitude lower than that of Wy 14,643 (Table 2), whereas the efficacy is comparable, suggesting that this compound is a full PPARα agonist. We also tested these compounds with the murine PPARα, and in this case Wy 14,643 is more potent than (*S*)-**1** (Table 2). The potency of (*S*)-**1** on the murine PPARα is comparable to that of the human, while the EC_{50} of Wy 14,643 with the murine receptor is much lower (Table 2). The *R*-enantiomer is not active on both human PPARα (Figure 2B and Table 2) and mouse PPARα (Table 2). Both the *R* and *S*-enantiomers activate PPARγ (Figure 2C), although their potency is significantly lower than that of the reference PPARγ agonist rosiglitazone (Table 2). Interestingly, transfected cells treated with (*S*)-**1** and (*R*)-**1** do not achieve full activation of PPARγ-dependent transcription (Figure 2C and Table 2), suggesting that these two compounds may be partial agonists of PPARγ.

Binding of (*S*)-1 to PPARγ-LBD. Figure 3A shows the unambiguous positioning of the *S*-enantiomer fitted into the electron density map calculated in the hydrophobic pocket of PPARγ. Figure 4 summarizes the binding interactions between the polar head of the *S*-enantiomer and the surrounding residues. One of the carboxylate oxygens can form a bifurcated H-bond with the Y473 OH and the H449 $N^{\varepsilon 2}$ groups; the latter group engages the ligand ether oxygen in a further H-bond. The other carboxylate oxygen is at H-bonding distances from H323 $N^{\varepsilon 2}$, Y473 OH, and S289 OH. The residues H323, Y473, H449, and S289 are generally involved in the canonical intermolecular H-bonding network in the presence of carboxylate containing ligands. Figure 5A shows the cavity where the diphenyl group of the *S*-enantiomer is deeply inserted, there forming several favorable hydrophobic interactions. The bottom of the cavity is delimited by the loop 11/12 and is contoured sidewise by H3 and H11.The diphenyl group there acts as a stabilization pivot between these helices and the loop 11/12. Inside the cavity, the diphenyl group interacts on one side with L453 and more weakly with I456 of H11 and interacts on the other side with the Q286 of H3. Favorable van der Waals contacts are also realized by the benzyl group and the asymmetric carbon atom of the *S*-enantiomer with the S289 OH group. At the bottom of the cavity, the terminal end of the diphenyl group faces the M463 side chain of the loop 11/12. The short contact between the distal aromatic ring and M463 is well evidenced by continuous electron density between the two interacting groups (see Supporting Information Figure1).

Conformational Change Induced by (*S*)-1 in the Hydrophobic Pocket of PPARγ. A comparison between the crystal complex PPARγ/(*S*)-**1** and PPARγ complexes (PDB codes 1FM9, 1K74, 1ZEO, 2GOG, 2GOH)[17−20] including ligands occupying the "benzophenone pocket", a contiguous region of the hydrophobic pocket formed by H3, H7, and H11, reveals a conformational change induced by (*S*)-**1** in the PPARγ-LBD. Figure 6 reports the superposition between the crystal complex of the *S*-enantiomer with that of farglitazar (PDB code 1FM9). There, it can be seen that the rigid and straight diphenyl group of the *S*-enantiomer induces a switching of the F282 side chain, from the extended conformation ($\chi^1 = 172°$), adopted in the PDB files cited above, to the folded g* conformation ($\chi^1 = -58°$). As a consequence, the F282 side chain turns to the benzophenone pocket, leaving free its previous position that is replaced by the distal ring of the *S*-enantiomer. In this way, the F282 side chain could function as a gate-keeper, rendering accessible a new region for accommodation of long and straight substituents of the ligand. The size and shape of this region have been evaluated by the program VOIDOO[21] (see Figure 7). The region is "L" shaped and the diphenyl group occupies the first branch, corresponding to about 50% of its entire volume (∼1016 Å^3). We propose to name this branch "diphenyl pocket" in analogy with the "benzophenone pocket". The diphenyl pocket is delimited at the bottom by the central part of the loop 11/12. In this way the distal aromatic ring of the ligand plays the key role, normally played by F282, in stabilizing the region

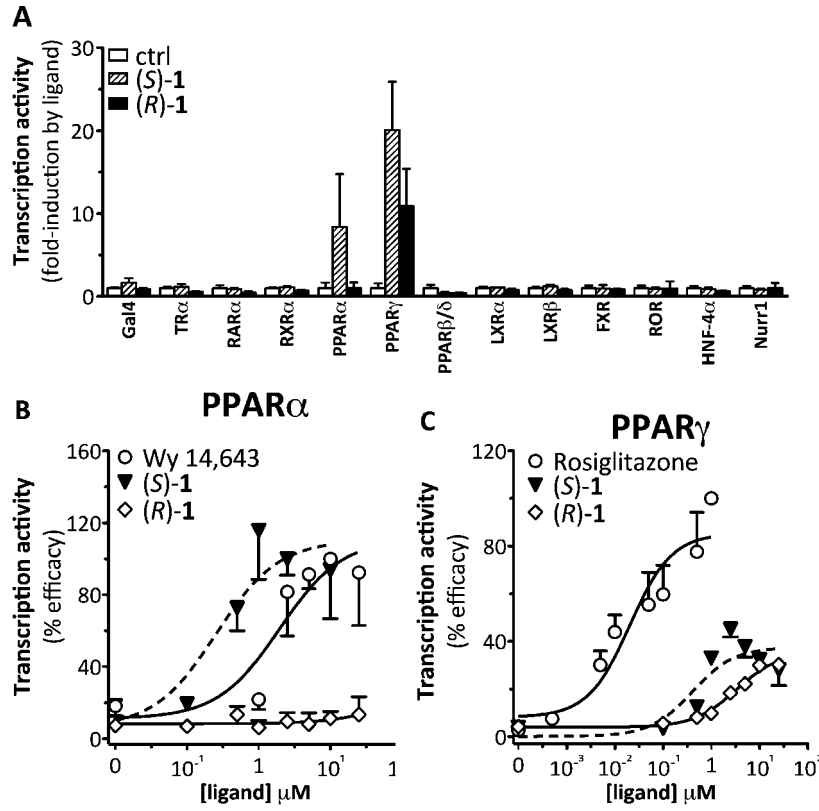

Figure 2. Transcription activity of **1**: (A) activity of (*S*)-**1** and (*R*)-**1** was tested toward a panel of nuclear receptor LBDs in a Gal4-based assay; (B, C) concentration−response curves of (*S*)-**1** and (*R*)-**1** with human (B) PPARα and (C) PPARγ. Results are expressed as a percentage of efficacy, and each point is the mean ± SEM of three to five independent experiments each performed in triplicate wells.

Table 1. Statistics of Crystallographic Data and Refinement

	PPARγ/(S)-1	PPARγ/(R)-1	PPARγ/(S)-2
wavelength (Å)	1.2	0.933	0.933
temperature (K)	100	100	100
space group	*C*2	*C*2	*C*2
no. of mol in the au	2	2	
cell axes (Å)	93.14, 61.57, 118.80	93.54, 61.05, 119.24	93.25, 60.98, 118.54
β angle (deg)	103.40	103.49	102.83
resolution range (Å)	20.00−2.60 (2.69−2.60)[a]	20.00−2.40 (2.53−2.40)[a]	20.00−2.65 (2.79−2.65)[a]
R_{merge} (%)	4.5 (36.6)[a]	9.4 (32.7)[a]	8.4 (48.6)[a]
multiplicity	4 (4)[a]	3.5 (3.3)[a]	3.7 (3.8)[a]
$I/\sigma(I)$	25.6 (3.4)[a]	4.8 (2.0)[a]	7.7 (1.4)[a]
completeness (%)	99.8 (99.7)[a]	98.4 (97.3)[a]	98.3 (98.1)[a]
R_{factor} (%)	24.8	24.8	24.1

[a] The values in parentheses refer to the outer shell.

Table 2. Potency and Efficacy of (*S*)-**1** and (*R*)-**1** toward PPARα and PPARγ As Determined in Gal4-Based Assays[a]

	hPPARγ		hPPARα		mPPARα	
tested ligand	EC_{50} (μM)	efficacy (%)	EC_{50} (μM)	efficacy (%)	EC_{50} (μM)	efficacy (%)
rosiglitazone	0.04 ± 0.02	100				
Wy 14,643			1.62 ± 0.34	100	0.04 ± 0.002	100
(*S*)-**1**	0.48 ± 0.08	35 ±6.5	0.22 ± 0.02	100±9.5	0.26 ± 0.06	120±11
(*R*)-**1**	5.93 ± 2.60	24 ±4.7	na	na	na	na

[a] Values are the mean ± SEM. Efficacy values were calculated as percentage of rosiglitazone (100%) for PPARγ and as percentage of Wy 14,643 (100%) for human and mouse PPARα. Values were calculated from three to five independent experiments each performed in triplicate. na: not active at the tested concentrations.

including this loop. It is well known that differences in the hydrophobic packing of this loop may contribute to different H12 dynamics.[22,23] This is the first structure of PPARγ in which such conformational change of the F282 side chain has been observed. A similar conformational change induced by the ligand is also present in the crystal complex between the PPARα-LBD and the azetidinone derivative PPARα/γ dual agonist BSM631707 (PDB code 2REW).[24] This ligand forces the side chain of F273, equivalent to F282 in PPARγ, to a folded conformation that allows the accommodation of its terminal end.

In this regard, we solved the crystal structure of the complex of PPARγ-LBD with the previously reported[16] PPARα/γ dual agonist (*S*)-**2**, structurally related to (*S*)-**1**, only differing in the ethyl group replacing the distal aromatic ring of (*S*)-**1** (see Figure 8).

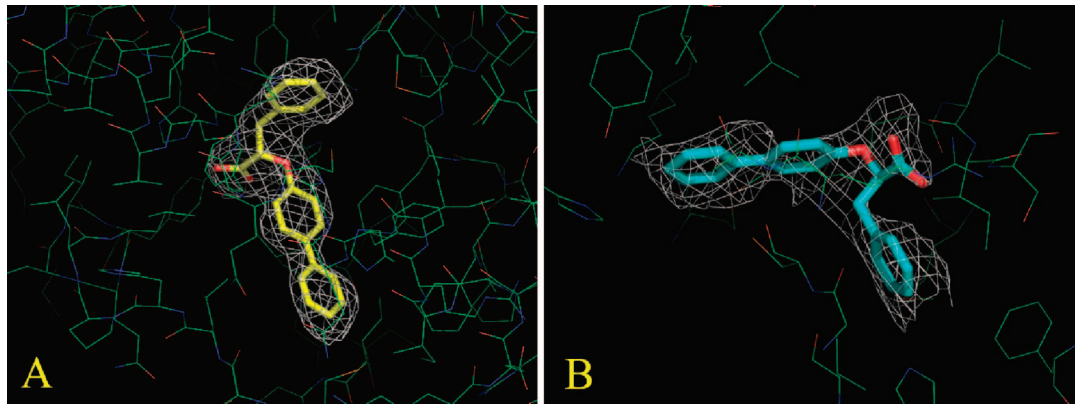

Figure 3. $2F_o - F_c$ electron density maps calculated around (A) (*S*)-**1** and (B) (*R*)-**1**. All the maps are contoured at 1σ.

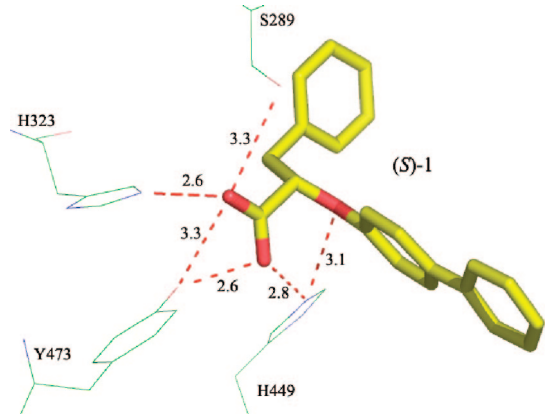

Figure 4. Hydrogen bond network of (*S*)-**1** in complex with PPARγ.

Also, in this case the conformational change of the F282 side chain induced by the ligand (see Supporting Information Figure 2a,b) has been observed. It could be argued that even the presence of small substituents in the para position of the phenoxy group of (*S*)-**1** could provoke the rearrangement of F282 side chain.

Since (*S*)-**1** occupies only the first branch of the new L-shaped region, we decided to start the preparation of some analogues characterized from the presence on the diphenyl system of groups that could allow the complete occupation of the entire cavity with the aim of evaluating the effects due to a further stabilization of H11, H12, and the loop 11/12 in terms of potency, efficacy, and subtype selectivity. At the present, only the (*S*)-**3** and (*S*)-**4** analogues reported in Figure 8 have been synthesized and evaluated for their PPARα/γ activity. These compounds were prepared similarly to (*S*)-**1** (all synthetic details will be reported elsewhere) and are characterized from an increased flexibility due to the presence of one or two methylenic groups between the phenyl rings of (*S*)-**1** which in our mind could allow the accommodation of the distal aromatic ring inside the second branch of the L-shaped region. However, the results do not show any significant modification of the activity on PPARγ ($EC_{50} = 0.57 \pm 0.01$ μM, efficacy = 40% ± 4% for (*S*)-**3**; $EC_{50} = 0.40 \pm 0.20$ μM, efficacy = 33% ± 5% for (*S*)-**4**) and only an increased potency of PPARα activation for (*S*)-**3** ($EC_{50} = 0.011 \pm 0.002$ μM, efficacy = 107% ± 5% for (*S*)-**3**; $EC_{50} = 0.15 \pm 0.04$ μM, efficacy = 83% ± 10% for (*S*)-**4**). The interpretation of these results by X-ray structure analysis of the complexes of these new ligands with PPARγ-LBD is in progress.

Binding of (*R*)-1 to PPARγ-LBD. Figure 3B represents the *R*-enantiomer fitted into the $2F_o - F_c$ electron density map. Figure 5B shows a C^α superposition of the complexes PPARγ/(*S*)-**1** and PPARγ/(*R*)-**1**. Inside the cavity, (*R*)-**1** occupies a different region with respect to (*S*)-**1**, between H3 and the β-sheet. In this way the polar head of (*R*)-**1** cannot form the usual network of H-bonds with H323, H449, and Y473, and it does not interact at all with H11 and H12. The carboxylate group of (*R*)-**1** forms one H-bond with S342 NH of the β-sheet and engages the charged R288 residue of H3 in an electrostatic interaction. Obviously, the positioning of (*R*)-**1** in a different region of the cavity leaves the F282 side chain in its usual conformation. The position of (*R*)-**1** is similar to that of the partial agonists nTZDpa and BVT.13 in the complexes with PPARγ (PDB codes 2Q5S and 2Q6S);[25,26] also in that case these compounds formed a H-bond with the NH of S342.

Molecular Mechanism of Partial Agonism. (*S*)-**1** is a PPARα/γ dual agonist that shows full agonism on PPARα (Figure 2A and Table 2) and partial agonism on PPARγ (see Figure 2C and Table 2). To explain this different subtype behavior, we have docked (*S*)-**1** into the PPARα-LBD and we have superimposed the putative complex with the crystal complex PPARγ/(*S*)-**1**, as shown in Figure 9A. The polar head of the ligand in the complex with PPARα is shifted of about 1.5 Å toward H3 with respect to the position adopted in the crystal complex of PPARγ. This shift is caused by the longer protrusion of the Y314 side chain of PPARα, equivalent to H323 of PPARγ. As a consequence, the diphenyl group adopts a slope different from that observed in the crystal complex of PPARγ, approaching H11 more closely and partially losing interactions with H3. The favorable van der Waals contacts between the diphenyl group and residues belonging to H11 of PPARα are the following: 3.6 and 2.9 Å, respectively, with C^α and CO of V444, 3.4 Å with the side chain of I447, and 3.4 Å with C^α of K448 (see Figure 9B). These contacts, together with that realized with the loop 11/12, better stabilize the contiguous H12, with a consequent improvement of the efficacy of the ligand toward PPARα. On the other hand, the partial agonism of the *S*-enantiomer toward PPARγ can be attributed to a lower stabilization of H11 and increased stabilization of H3, as before discussed.

In order to check the interaction pattern of (*S*)-**1** with H3 and H11 of both PPARα and PPARγ, we carried out MD simulations in water solution at 300 K. In this regard, we considered as an interacting couple, two noncovalently bonded atoms experiencing a contact shorter than 3.9 Å with a probability not lower than 0.37, corresponding to a negative free energy of formation at 300 K. The result, schematically

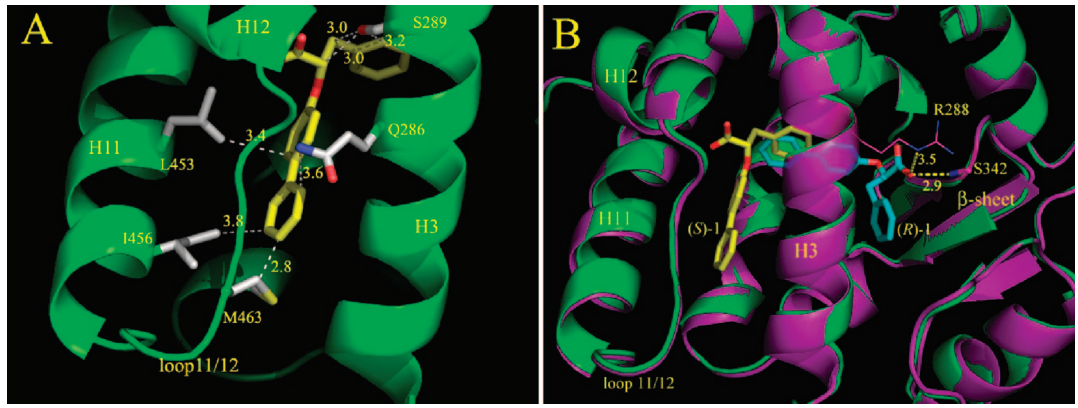

Figure 5. (A) Hydrophobic interactions of (*S*)-**1** in the PPARγ internal cavity; (B) C$^{\alpha}$ superposition of the complexes of PPARγ with (*S*)-**1** (yellow) and (*R*)-**1** (cyan). H-bonds and electrostatic interactions of (*R*)-**1** are shown by dashed lines.

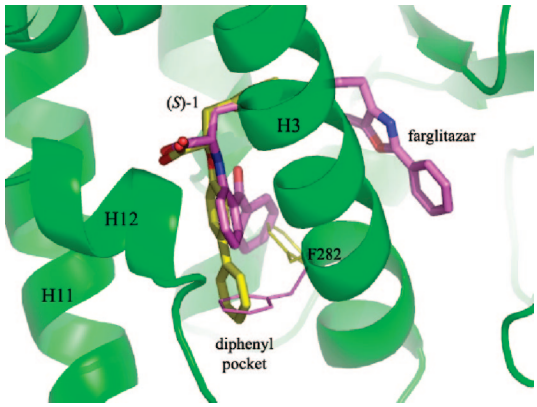

Figure 6. C$^{\alpha}$ superposition of the complexes of PPARγ with (*S*)-**1** (yellow) and farglitazar (pink). For clarity only the cartoon of PPARγ/(*S*)-**1** is shown (green). The orientation of F282 in the two complexes is also shown (colored as the correspondent ligand).

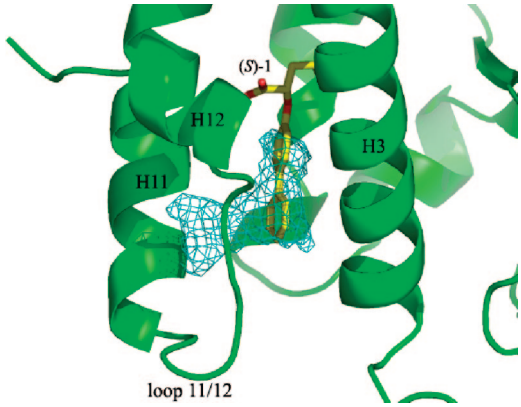

Figure 7. New cavity calculated by VOIDOO (blue-colored mesh). (*S*)-**1** is shown in yellow.

reported in Figure 10, confirms that (*S*)-**1** interacts with both H3 and H11 of PPARα and only with H3 of PPARγ.

In order to also evaluate the mechanical stabilization caused by the above interactions, we focused our attention on the change of the root mean square fluctuation (RMSF) of these helices, upon complexation with PPARα and PPARγ. As a result, we observed very low RMSF of both helices in the apo form of PPARα, the result being practically unaffected upon complexation. For PPARγ we registered a limited but clear reduction of the RMSF, from 1.0 $\pm$ 0.2 Å (apo form) to 0.7 $\pm$ 0.2 Å (complexed form) for H3. A rather low RMSF (0.3 $\pm$ 0.2 Å) characterizes H11 of both apo and complexed forms (see Supporting Information Figure 3a,b).

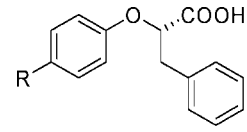

(*S*)-2: R = CH_2CH_3
(*S*)-3: R = CH_2Ph
(*S*)-4: R = CH_2CH_2Ph

Figure 8. Chemical structures of the (*S*)-**1** analogues, (*S*)-**2**, (*S*)-**3**, and (*S*)-**4**.

Moreover, the analysis of the average distances between the carboxylate oxygens of the ligand and the N$^{\varepsilon 2}$ of H449, the N$^{\varepsilon 2}$ of of H323, the OH of Y473, and the OH of S289 (N$^{\varepsilon 2}$ of H440, OH of Y314, Y464, and S280, respectively, in PPARα) shows that in the MD simulation of the PPARγ complex only the H-bond with Y473 is maintained, whereas in the PPARα complex all the H-bonds are maintained during the simulation (see Supporting Information Figures 4−11). Thus, the partial agonism of (*S*)-**1** could also be ascribed to the weakening of significant H-bonds involving the carboxylate of the ligand with some conserved residues of the protein, particularly that with H449 of H11.

Recently, H/D exchange kinetics and X-ray experiments have been performed for six complexes of PPARγ with full and partial agonists.[25] On the basis of the structures of their complexes, ligands were broadly grouped into those that occupy the portion of LBD spanning from H11 and H12 beyond H3 to those that occupy the region between H3 and the β-sheet. Among the compounds of the first class, stronger transcriptional efficacy was achieved with an increased stabilization of H12 and a corresponding decrease of stabilization of H3. The compounds of this class with weaker transactivation profiles (like the *S*-enantiomer here described) preferentially stabilize H3 through closer hydrophobic contacts or H-bonds made with residues of this helix. This relationship is in agreement with our previous findings regarding two enantiomeric ureidofibrate derivatives complexed with PPARγ, showing partial and full agonism, respectively, toward this nuclear receptor.[27] Even in that case, while the full agonism of one enantiomer could be related to stronger interactions with H11, H12, and the loop 11/12, the partial agonism of the other enantiomer could be ascribed to closer contacts with a residue (Q286) of H3. Compound (*R*)-**1** belongs to the second class of PPARγ ligands; compounds belonging to this class differentially stabilize other

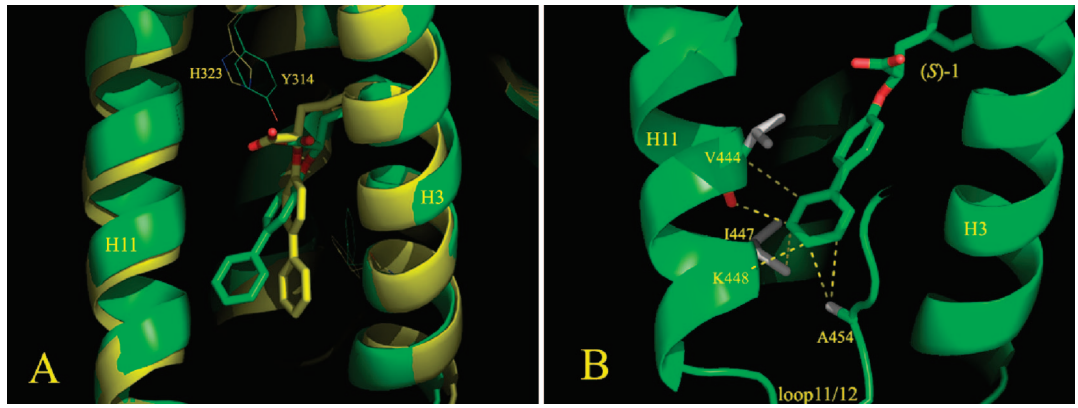

Figure 9. (A) C^{α} superposition of PPARγ and PPARα LBD. (*S*)-**1** is respectively complexed with PPARγ (yellow) and docked in the PPARα LBD (green). (B) Binding pose of (*S*)-**1** (green) into the PPARα LBD as calculated by Gold software.[35] The more favorable hydrophobic interactions are also shown.

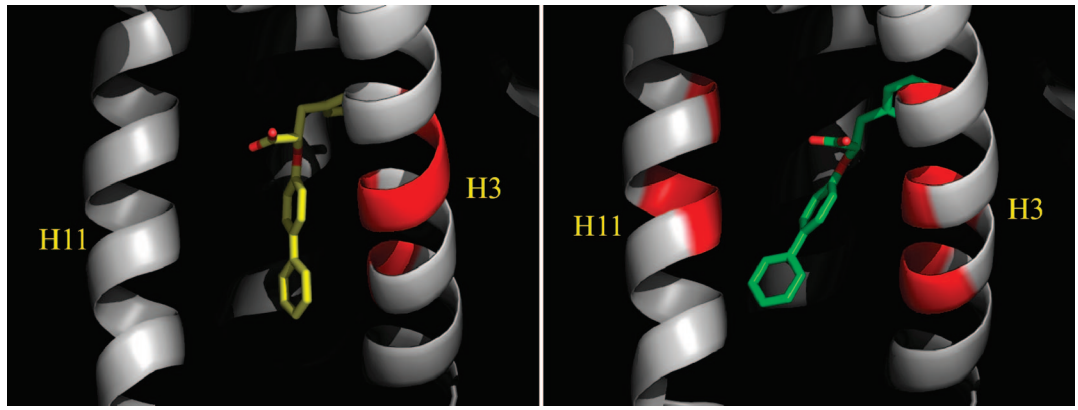

Figure 10. Interaction pattern of (*S*)-**1** with H3 and H11 (A) in complex with PPARγ and (B) in complex with PPARα. Residues of H3 and H11 interacting with the ligand at distances shorter than 3.9 Å are colored red. (*S*)-**1**, respectively complexed with PPARγ (yellow) and docked in the PPARα LBD (green), is also shown.

regions of LBD rather than H12, for example, the β-sheet and H3, with modest transactivation profiles (efficacy of <50%). It has also been proposed that this differential stabilization could suggest a distinct coactivator-binding surface, consistent with the findings that regions outside the LxxLL motifs contribute to receptor binding.[28] Finally, the potency of (*R*)-**1** is lower than that of (*S*)-**1** on the same receptor. This behavior can be easily interpreted at the molecular level by the bindings found in the relative complexes here reported. While (*S*)-**1** forms direct H-bonding interactions with H12, (*R*)-**1** does not interact at all with the active helix.

Conclusions

New drug design strategies should be considered when docking ligands on PPARs in light of the data here reported. In fact, the F282 side chain conformation in PPARγ can be changed, rendering accessible a new region never explored before. Moreover, since (*S*)-**1** occupies only the first branch of this new region, it is evident that additional space is available for bulkier substituents protruding toward H11 and H12. The complete occupation of the entire cavity would confer a further stabilization of H11, H12, and the loop 11/12 and could affect potency, efficacy, and PPARα/PPARγ selectivity. This is an important point, as the design of new molecules occupying this pocket may provide the opportunity to modulate the receptor activity via the selective recruitment of coactivators that confer beneficial effects but avoid at the same time the typical side effects observed with known PPARγ ligands. The preliminary results obtained with two (*S*)-**1** analogues endowed with increased flexibility do not show remarkable change of PPARγ activity; however, more structural modifications are needed for an appropriate evaluation of this matter. For this purpose, the preparation of new derivatives characterized by the presence on the diphenyl system of groups with different stereoelectronic properties is under way. A molecular mechanism not only considering the stabilization of H12 but including even the increased stabilization of H3 and the β-sheet has been elucidated for the coactivator recruitment to the receptor in response to ligands showing graded transcriptional responses. MD simulations in water solution also showed that the possible weakening of significant H-bonds realized by the ligand could be responsible for its different subtype behavior.

Experimental Section

Chemical Methods. Column chromatography was performed on ICN silica gel 60 Å (63−200 μm) as the stationary phase. Melting points were determined in open capillaries on a Gallenkamp electrothermal apparatus and are uncorrected. Mass spectra were recorded with a HP GC/MS 6890-5973 MSD spectrometer, electron impact 70 eV, equipped with an HP chemstation. ^{1}H NMR spectra were recorded in $CDCl_3$ on a Varian-Mercury 300 (300 MHz) spectrometer. Chemical shifts are expressed as parts per million (δ). Microanalyses of solid compounds were carried out with an Eurovector Euro EA 3000 model analyzer; the analytical results are within ±0.4% of theoretical values. Optical rotations were measured with a Perkin-Elmer 341 polarimeter at room temperature (20 °C): concentrations are expressed as g/(100 mL). The enan-

tiomeric excesses of acids were determined by HPLC analysis of their methyl esters, obtained by reaction with an ethereal solution of diazomethane, on a Chiralcel OD column (4.6 mm i.d. × 250 mm, Daicel Chemical Industries, Ltd., Tokio, Japan). Analytical liquid chromatography was performed on a PE chromatograph equipped with a Rheodyne 7725i model injector, a 785A model UV/vis detector, a series 200 model pump, and an NCI 900 model interface. Chemicals were from Aldrich and were used without any further purification.

Preparation of (*S*)-Methyl 2-(4-Phenylphenoxy)-3-phenylpropanoate. To an ice-bath cooled suspension of triphenylphosphine-PS (DVB 2%, 3 mmol·g^{-1}, 0.460 g, 1.380 mmol) in anhydrous toluene (5 mL) was added dropwise a solution of diisopropylazodicarboxylate (DIAD, 0.273 g, 1.350 mmol) in anhydrous toluene (5 mL). The resulting mixture was stirred for 0.5 h. A solution of (*R*)-methyl phenyllactate (0.201 g, 1.095 mmol) in anhydrous toluene (5 mL) and 4-phenylphenol (0.173 g, 1.016 mmol) was added at room temperature. The reaction mixture was stirred at room temperature overnight, the solid was filtered off, and the filtrate was evaporated to dryness to give a white residue. The title compound was purified by chromatography on silica gel column (petroleum ether/ethyl acetate 9:1 as eluents), obtaining a white solid (0.329 g, 0.991 mmol) in 97% yield. GC/MS, *m/z*: 332 (M^+, 100). ^{1}H NMR ($CDCl_3$): δ 3.26−3.29 (m, 2H, CH_2), 3.74 (s, 3H, CH_3), 4.83−4.88 (dd, 1H, CH), 6.89−7.53 (m, 14H, aromatics).

The *R*-enantiomer was prepared following the same procedure, starting from (*S*)-methyl phenyllactate, in 95% yield.

(−)-(*S*)-2-(4-Phenylphenoxy)-3-phenylpropanoic Acid. A solution of the methyl ester (0.301 g, 0.907 mmol) in THF (5 mL) and 1 N NaOH (5 mL) was stirred at room temperature for 4 h. The organic layer was removed under reduced pressure, and the residue was acidified with 6 N HCl and extracted with Et_2O. The organic layer was dried over Na_2SO_4 and evaporated to dryness, affording the final acid as a white solid that was recrystallized from hexane in 84% yield (0.242 g, 0.761 mmol). ^{1}H NMR ($CDCl_3$): δ 3.22−3.38 (m, 2H, CH_2), 4.84−4.94 (m, 1H, CH), 5.70 (bs, 1H, COOH, D_2O exchanged), 6.88−7.60 (m, 14H, aromatics). Mp 149−50 °C; $[\alpha]_D$ −1 (*c* 1.0, MeOH); 99% ee (methyl ester on Chiralcel OD column, hexane/*i*-PrOH 98:2 as the mobile phase, flow rate of 0.5 mL/min, detection at 230 nm).

(+)-(*R*)-2-(4-Phenylphenoxy)-3-phenylpropanoic Acid. Yield, 81%; mp 148−9 °C; $[\alpha]_D$ +1 (*c* 1.0, MeOH); 98% ee (methyl ester on Chiralcel OD column, hexane/*i*-PrOH 98:2 as the mobile phase, flow rate of 0.5 mL/min, detection at 230 nm).

Cell-Based Transcription Assay. The expression vectors for PPARα, PPARγ, and PPARβ/δ LBD fused in frame with the Gal4 DNA binding domain (pGal4-PPARαLBD, pGal4-PPARγLBD, pGal4-PPARβ/δLBD, respectively) and the reporter vector containing five copies of the Gal4 upstream activating sequences (pGal4UAS-luciferase) driving the transcription of the luciferase reporter gene were kind gifts from Krister Bamberg (AstraZeneca, Mölndal, Sweden). pCMVβ, containing the *E. coli* β-galactosidase gene driven by the cytomegalovirus early promoter/enhancer (Clontech, Mountain View, CA) was used as an internal standard to normalize for transfection efficiency across wells. All other vectors expressing Gal4 fusion proteins with the ligand binding domains of tested nuclear receptors have been described previously.[27] Cell-based transcription assays were performed by transfecting HepG2 cells with 100 ng of pGal4UAS-luciferase along with 50 ng of receptor vector and 300 ng of pCMVβ with the calcium phosphate coprecipitation technique for 4 h as described.[16] After removal of the DNA coprecipitates, cells were washed with phosphate-buffered saline and refed with serum-free medium (Dulbecco's modified Eagle medium/F-12 nutrient 1:1, Invitrogen, Milano, Italy) containing 100 U of penicillin G/mL and 100 μg of streptomycin sulfate/mL and the indicated concentrations of tested ligands or vehicle (0.1% ethanol). After 20 h, cells were harvested and luciferase and β-galactosidase activities were measured as described.[16] All transfection experiments were repeated at least three times. EC_{50} values for all tested ligands were calculated by using GraphPad Prism, version 5.0a, for Macintosh (GraphPad Software, San Diego, CA, www.graphpad.com).

Protein Expression, Purification, and Crystallization. The LBD of PPARγ was expressed as N-terminal His-tagged protein using a pET28 vector and purified as previously described.[27] Crystals of apo-PPARγ were obtained by vapor diffusion at 20 °C using the sitting drop made by mixing 2 μL of protein solution (15 mg/mL in 20 mM Tris, DTT 5 mM, 0.5 mM EDTA, pH 8.0) with 2 μL of reservoir solution (0.8 M Na citrate, 0.15 mM Tris, pH 8.0). The crystals were soaked for 3 days in a storage solution (1.2 M Na citrate, 0.15 M Tris, pH 8.0) containing the ligands (0.5 mM). The ligands dissolved in ethanol were diluted in the storage solution so that the final ethanol concentration was 1%. The storage solution with glycerol 20% (v/v) was used as cryoprotectant. Crystals of PPARγ/(*S*)-**1**, PPARγ/(*R*)-**1**, and PPARγ/(*S*)-**2** all belong to the space group *C*2 with cell parameters shown in Table 1. The asymmetric unit is formed by one homodimer (53.5% solvent for all complexes).

Structure Determination. X-ray data were collected at 100 K under a nitrogen stream using synchrotron radiation (beamline XRD1 at Elettra, Trieste, Italy, for the complex PPARγ/(*S*)-**1**; beamline ID14-1 at ESRF, Grenoble, France, for the other complexes). The diffracted intensities were processed using the programs DENZO and SCALEPACK[29] for the complex PPARγ/(*S*)-**1** and using MOSFLM and SCALA[30] for the other complexes. Refinements were performed with CNS[31] using the coordinates of apo-PPARγ[32] (PDB code 1PRG) as a starting model. All data between 8 and 2.6 Å were included for PPARγ/(*S*)-**1** (between 8 and 2.4 Å for PPARγ/(*R*)-**1**; between 8 and 2.4 Å for PPARγ/(*S*)-**2**). The statistics of crystallographic data and refinement are summarized in Table 1. The coordinates of PPARγ/(*S*)-**1**, PPARγ/(*R*)-**1**, and PPARγ/(*S*)-**2** complexes have been deposited in the Brookhaven Protein Data Bank (PDB) with the codes 3B3K, 3D6D, and 3CDS, respectively.

Computational Chemistry. Molecular modeling and graphics manipulations were performed using the molecular operating environment (MOE)[33] running on a 2 CPU (PIV 2.0−3.0 GHz) Linux workstation. Energy minimizations were realized by employing the AMBER 9 program,[34] selecting the parm99 force field.[35]

Model building and geometry optimizations of (*S*)-**1** enantiomer were accomplished with the MMFF94X force field, available within MOE. The carboxylate group was taken as dissociated. The coordinates of PPARα in the complex with the α/γ dual agonist BSM631707 (PDB code 2REW)[24] were used in the docking experiments. Bound ligand and water molecules were removed. A correct atom assignment for N, Q, and H residues was done, and hydrogen atoms were added using standard MOE geometries. Partial atomic charges were computed by MOE using the AMBER99 force field. All heavy atoms were then fixed, and hydrogen atoms were minimized using the AMBER99 force field and a constant dielectric of 1, terminating at a gradient of 0.001 kcal mol^{-1} Å^{-1}.

Enantiomer (*S*)-**1** was docked into the active site of PPARα using the GOLD 3.2 program,[36] computing interaction energies within a sphere of a 18 Å radius centered on the OH atom of Y464 in the PPARα structure. The poses obtained with the original Goldscore function are rescored and reranked with the GOLD implementation of the CHEMscore function. To perform a thorough and unbiased search of the conformation space, each docking run was allowed to produce 30 poses without the option of early termination, using standard default settings. In this docking run, the 30 poses produced by GOLD resulted in only one cluster on the basis of their conformations. The top solution (CHEMscore fitness = 41.2 kJ/mol) obtained after reranking of the poses with CHEMscore was selected to generate the PPARα/(*S*)-**1** complex.

To eliminate any residual geometric strain, the obtained complex was energy-minimized for 5000 steps using combined steepest descent and conjugate gradient methods until a convergence value of 0.001 kcal/(mol Å). Upon minimization, the protein backbone atoms were held fixed. The geometry optimization was performed using the SANDER module in the AMBER suite of programs, employing the Cornell et al. force field to assign parameters for

the standard amino acids. General AMBER force field (GAFF) parameters were assigned to ligands, while the partial charges were calculated using the AM1-BCC method as implemented in the ANTECHAMBER suite of AMBER.

Molecular Dynamics (MD) simulations of PPARγ/(*S*)-**1** and PPARα/(*S*)-**1** were carried out in aqueous solution according to the following protocol.

The complexes were put at the center of a box of 7.2 × 7.6 × 7.6 nm^3 volume. As starting structures, we considered the complex formed by docking (*S*)-**1** into the PPARα-LBD, and the crystal complex of PPARγ/(*S*)-**1**. The box was then filled with 11 476 Single Point Charges[37] water molecules to reproduce the typical liquid density. The electrical neutrality of the systems was ensured by adding the proper number of positive (Na^+) counterions, i.e., seven for PPARγ/(*S*)-**1** and two for PPARα/(*S*)-**1**. The same conditions were applied for simulating apo-PPARγ and apo-PPARα. All the simulations were initiated with a steepest descent optimization and solvent relaxation. Subsequently, a slow heating from 10 to 300 K was performed using short simulations of 50.0 ps. The simulations were then propagated for 13 ns in a NVT ensemble using an integration step of 2.0 fs with the rototranslational constraint applied to the solute.[38] The temperature was kept constant by the isokinetic temperature coupling,[39] and all bond lengths were constrained by adopting the LINCS algorithm.[40] Long range electrostatics was computed by the particle mesh Ewald (PME) method,[41] with 34 wave vectors in each dimension and a fourth-order cubic interpolation. The Gromos force field[42] was used for the protein, at neutral pH, and for (*S*)-**1**. The point charges of the latter were calculated with a standard fitting scheme[43] carried out on density functional theory calculations using the Becke3LYP functional[44] with 6-311+g(d) basis set using the Gaussian 03 package.[45] The Gromacs software[46] was employed for all the MD runs.

Statistical evaluations on selected observables were calculated by dividing the trajectory in two subparts and reporting the semidispersion around the average value.

Acknowledgment. The authors acknowledge CASPUR (Roma) for the use of Gaussian 03.

Supporting Information Available: X-ray and molecular dynamics data. This material is available free of charge via the Internet at http://pubs.acs.org.

References

(1) Berger, J.; Moller, D. E. The mechanisms of action of PPARs. *Annu. Rev. Med.* **2002**, *53*, 409–435.
(2) Berger, J. P.; Akiyama, T. E.; Meinke, P. T. PPARs: therapeutic targets for metabolic disease. *Trends Pharmacol. Sci.* **2005**, *26* (5), 244–251.
(3) Kliewer, S. A.; Sundseth, S. S.; Jones, S. A.; Brown, P. J.; Wisely, G. B.; Koble, C. S.; Devchand, P.; Wahli, W.; Willson, T. M.; Lenhard, J. M.; Lehmann, J. M. Fatty acids and eicosanoids regulate gene expression through direct interactions with peroxisome proliferator-activated receptors alpha and gamma. *Proc. Natl. Acad. Sci. U.S.A.* **1997**, *94* (9), 4318–4323.
(4) Nagy, L.; Schwabe, J. W. Mechanism of the nuclear receptor molecular switch. *Trends Biochem. Sci.* **2004**, *29* (6), 317–324.
(5) Nettles, K. W.; Greene, G. L. Ligand control of coregulator recruitment to nuclear receptors. *Annu. Rev. Physiol.* **2005**, *67*, 309–333.
(6) Renaud, J. P.; Moras, D. Structural studies on nuclear receptors. *Cell. Mol. Life Sci.* **2000**, *57* (12), 1748–1769.
(7) Desvergne, B.; Wahli, W. Peroxisome proliferator-activated receptors: nuclear control of metabolism. *Endocr. Rev.* **1999**, *20* (5), 649–688.
(8) Issemann, I.; Prince, R. A.; Tugwood, J. D.; Green, S. The peroxisome proliferator-activated receptor:retinoid X receptor heterodimer is activated by fatty acids and fibrate hypolipidaemic drugs. *J. Mol. Endocrinol.* **1993**, *11* (1), 37–47.
(9) Rubins, H. B.; Robins, S. J.; Collins, D.; Fye, C. L.; Anderson, J. W.; Elam, M. B.; Faas, F. H.; Linares, E.; Schaefer, E. J.; Schectman, G.; Wilt, T. J.; Wittes, J. Gemfibrozil for the secondary prevention of coronary heart disease in men with low levels of high-density lipoprotein cholesterol. Veterans Affairs High-Density Lipoprotein Cholesterol Intervention Trial Study Group. *N. Engl. J. Med.* **1999**, *341* (6), 410–418.
(10) Gangloff, M.; Ruff, M.; Eiler, S.; Duclaud, S.; Wurtz, J. M.; Moras, D. Crystal structure of a mutant hERalpha ligand-binding domain reveals key structural features for the mechanism of partial agonism. *J. Biol. Chem.* **2001**, *276* (18), 15059–15065.
(11) Lehmann, J. M.; Moore, L. B.; Smith-Oliver, T. A.; Wilkison, W. O.; Willson, T. M.; Kliewer, S. A. An antidiabetic thiazolidinedione is a high affinity ligand for peroxisome proliferator-activated receptor gamma (PPAR gamma). *J. Biol. Chem.* **1995**, *270* (22), 12953–12956.
(12) Hulin, B.; McCarthyP, A.; Gibbs, E. M. *Curr. Pharm. Des.* **1996**, *2*, 85–102.
(13) Grey, A. Skeletal consequences of thiazolidinedione therapy. *Osteoporosis Int.* **2008**, *19* (2), 129–137.
(14) Rubenstrunk, A.; Hanf, R.; Hum, D. W.; Fruchart, J. C.; Staels, B. Safety issues and prospects for future generations of PPAR modulators. *Biochim. Biophys. Acta* **2007**, *1771* (8), 1065–1081.
(15) Shearer, B. G.; Billin, A. N. The next generation of PPAR drugs: do we have the tools to find them? *Biochim. Biophys. Acta* **2007**, *1771* (8), 1082–1093.
(16) Pinelli, A.; Godio, C.; Laghezza, A.; Mitro, N.; Fracchiolla, G.; Tortorella, V.; Lavecchia, A.; Novellino, E.; Fruchart, J. C.; Staels, B.; Crestani, M.; Loiodice, F. Synthesis, biological evaluation, and molecular modeling investigation of new chiral fibrates with PPARalpha and PPARgamma agonist activity. *J. Med. Chem.* **2005**, *48* (17), 5509–5519.
(17) Gampe, R. T., Jr.; Montana, V. G.; Lambert, M. H.; Miller, A. B.; Bledsoe, R. K.; Milburn, M. V.; Kliewer, S. A.; Willson, T. M.; Xu, H. E. Asymmetry in the PPARgamma/RXRalpha crystal structure reveals the molecular basis of heterodimerization among nuclear receptors. *Mol. Cell* **2000**, *5* (3), 545–555.
(18) Xu, H. E.; Lambert, M. H.; Montana, V. G.; Plunket, K. D.; Moore, L. B.; Collins, J. L.; Oplinger, J. A.; Kliewer, S. A.; Gampe, R. T., Jr.; McKee, D. D.; Moore, J. T.; Willson, T. M. Structural determinants of ligand binding selectivity between the peroxisome proliferator-activated receptors. *Proc. Natl. Acad. Sci. U.S.A.* **2001**, *98* (24), 13919–13924.
(19) Shi, G. Q.; Dropinski, J. F.; McKeever, B. M.; Xu, S.; Becker, J. W.; Berger, J. P.; MacNaul, K. L.; Elbrecht, A.; Zhou, G.; Doebber, T. W.; Wang, P.; Chao, Y. S.; Forrest, M.; Heck, J. V.; Moller, D. E.; Jones, A. B. Design and synthesis of alpha-aryloxyphenylacetic acid derivatives: a novel class of PPARalpha/gamma dual agonists with potent antihyperglycemic and lipid modulating activity. *J. Med. Chem.* **2005**, *48* (13), 4457–4468.
(20) Lu, I. L.; Huang, C. F.; Peng, Y. H.; Lin, Y. T.; Hsieh, H. P.; Chen, C. T.; Lien, T. W.; Lee, H. J.; Mahindroo, N.; Prakash, E.; Yueh, A.; Chen, H. Y.; Goparaju, C. M.; Chen, X.; Liao, C. C.; Chao, Y. S.; Hsu, J. T.; Wu, S. Y. Structure-based drug design of a novel family of PPARgamma partial agonists: virtual screening, X-ray crystallography, and in vitro/in vivo biological activities. *J. Med. Chem.* **2006**, *49* (9), 2703–2712.
(21) Kleywegt, G. J.; Jones, T. A. *Acta Crystallogr.* **1994**, *D50*, 178–185.
(22) Nettles, K. W.; Sun, J.; Radek, J. T.; Sheng, S.; Rodriguez, A. L.; Katzenellenbogen, J. A.; Katzenellenbogen, B. S.; Greene, G. L. Allosteric control of ligand selectivity between estrogen receptors alpha and beta: implications for other nuclear receptors. *Mol. Cell* **2004**, *13* (3), 317–327.
(23) Hellal-Levy, C.; Fagart, J.; Souque, A.; Wurtz, J. M.; Moras, D.; Rafestin-Oblin, M. E. Crucial role of the H11−H12 loop in stabilizing the active conformation of the human mineralocorticoid receptor. *Mol. Endocrinol.* **2000**, *14* (8), 1210–1221.
(24) Wang, W.; Devasthale, P.; Farrelly, D.; Gu, L.; Harrity, T.; Cap, M.; Chu, C.; Kunselman, L.; Morgan, N.; Ponticiello, R.; Zebo, R.; Zhang, L.; Locke, K.; Lippy, J.; O'Malley, K.; Hosagrahara, V.; Zhang, L.; Kadiyala, P.; Chang, C.; Muckelbauer, J.; Doweyko, A. M.; Zahler, R.; Ryono, D.; Hariharan, N.; Cheng, P. T. Discovery of azetidinone acids as conformationally-constrained dual PPARalpha/gamma agonists. *Bioorg. Med. Chem. Lett.* **2008**, *18* (6), 1939–1944.
(25) Bruning, J. B.; Chalmers, M. J.; Prasad, S.; Busby, S. A.; Kamenecka, T. M.; He, Y.; Nettles, K. W.; Griffin, P. R. Partial agonists activate PPARgamma using a helix 12 independent mechanism. *Structure* **2007**, *15* (10), 1258–1271.
(26) Ostberg, T.; Svensson, S.; Selen, G.; Uppenberg, J.; Thor, M.; Sundbom, M.; Sydow-Backman, M.; Gustavsson, A. L.; Jendeberg, L. A new class of peroxisome proliferator-activated receptor agonists with a novel binding epitope shows antidiabetic effects. *J. Biol. Chem.* **2004**, *279* (39), 41124–41130.
(27) Pochetti, G.; Godio, C.; Mitro, N.; Caruso, D.; Galmozzi, A.; Scurati, S.; Loiodice, F.; Fracchiolla, G.; Tortorella, P.; Laghezza, A.; Lavecchia, A.; Novellino, E.; Mazza, F.; Crestani, M. Insights into the mechanism of partial agonism: crystal structures of the peroxisome proliferator-activated receptor gamma ligand-binding domain in the complex with two enantiomeric ligands. *J. Biol. Chem.* **2007**, *282* (23), 17314–17324.

(28) Klein, F. A.; Atkinson, R. A.; Potier, N.; Moras, D.; Cavarelli, J. Biochemical and NMR mapping of the interface between CREB-binding protein and ligand binding domains of nuclear receptor: beyond the LXXLL motif. *J. Biol. Chem.* **2005**, *280* (7), 5682–5692.
(29) Otwinowski, Z.; Minor, W. *Methods Enzymol.* **1997**, *276*, 307–326.
(30) Leslie, A. G. W. *Joint CCP4 ESF-EACMB Newsletters Protein Crystallogr.* **1992**, 26.
(31) Brunger, A. T.; Adams, P. D.; Clore, G. M.; DeLano, W. L.; Gros, P.; Grosse-Kunstleve, R. W.; Jiang, J. S.; Kuszewski, J.; Nilges, M.; Pannu, N. S.; Read, R. J.; Rice, L. M.; Simonson, T.; Warren, G. L. Crystallography & NMR system: a new software suite for macromolecular structure determination. *Acta Crystallogr., Sect. D: Biol. Crystallogr.* **1998**, *54* (Part 5), 905–921.
(32) Nolte, R. T.; Wisely, G. B.; Westin, S.; Cobb, J. E.; Lambert, M. H.; Kurokawa, R.; Rosenfeld, M. G.; Willson, T. M.; Glass, C. K.; Milburn, M. V. Ligand binding and co-activator assembly of the peroxisome proliferator-activated receptor-gamma. *Nature* **1998**, *395* (6698), 137–143.
(33) *Molecular Operating Environment (MOE)*, version 2005.06; Chemical Computing Group, Inc.: Montreal, Canada, 2005.
(34) Case, D. A. e. a. *AMBER 9*; University of California: San Francisco, CA, 2006.
(35) Cornell, W. D.; Cieplak, P.; Bayly, C. I.; Gould, I. R.; Merz, K. M., Jr.; Ferguson, D. M.; Spellmeyer, D. C.; Fox, T.; Caldwell, J. W.; Kollman, P. A. *J. Am. Chem. Soc.* **1995**, *117*, 5179–5197.
(36) Jones, G.; Willett, P.; Glen, R. C.; Leach, A. R.; Taylor, R. Development and validation of a genetic algorithm for flexible docking. *J. Mol. Biol.* **1997**, *267* (3), 727–748.
(37) Berendsen, H. J. C.; Postma, J. P. M.; van Gunsteren, W. F.; Hermans, J. Interaction Models for Water in Relation to Protein Hydration. In *Intermolecular Forces*; Pullman, B., Ed.; D. Reidel Publishing Company: Dordrecht, The Netherlands, 1981; pp 331−342.
(38) Amadei, A.; Chillemi, G.; Ceruso, M.; Grottesi, A.; Di Nola, A. Molecular dynamics simulations with constrained roto-translational motions: theoretical basis and statistical mechanical consistency. *J. Chem. Phys.* **2000**, *112*, 9–23.
(39) Evans, D. J.; Morris, G. P. *Statistical Mechanics of Nonequilibrium Liquids*; Academic Press: London, 1990.
(40) Hess, B.; Bekker, H.; Berendsen, H. J. C.; Frajie, J. G. E. M. LINCS: a linear constraint solver for molecular simulations. *J. Comput. Chem.* **1997**, *18*, 1463–1472.
(41) Darden, T. A.; York, D. M.; Pederse, L. J. Particle mesh Ewald: method for Ewald sums in large systems. *J. Chem. Phys.* **1993**, *98*, 10089–10092.
(42) van Gunsteren, W. F.; Billeter, S. R.; Eising, A. A.; Hunemberger, P. H.; Kruger, P.; Mark, A. E.; Scott, V. R. P.; Tironi, I. G. *Biomolecular Simulations: The GROMOS96 Manual and User Guide*; vdf Hochschlverlag AG an der ETH Zurich: Zurich, Switzerland, 1996.
(43) Breneman, C. M.; Wiberg, K. B. Determining atom-centered monopoles from molecular electrostatic potentials. *J. Comput. Chem.* **1990**, *11*, 361–367.
(44) Parr, R. G.; Yang, W. *Density functional Theory of Atoms and Molecules*; Oxford University Press: New York, 1989.
(45) Frisch, M. J.; Trucks, G. W.; Schlegel, H. B.; Scuseria, G. E.; Robb, M. A.; Cheeseman, J. R.; Montgomery, J. A., Jr.; Vreven, T.; Kudin, K. N.; Burant, J. C.; Millam, J. M.; Iyengar, S. S.; Tomasi, J.; Barone, V.; Mennucci, B.; Cossi, M.; Scalmani, G.; Rega, N.; Petersson, G. A.; Nakatsuji, H.; Hada, M.; Ehara, M.; Toyota, K.; Fukuda, R.; Hasegawa, J.; Ishida, M.; Nakajima, T.; Honda, Y.; Kitao, O.; Nakai, H.; Klene, M.; Li, X.; Knox, J. E.; Hratchian, H. P.; Cross, J. B.; Bakken, V.; Adamo, C.; Jaramillo, J.; Gomperts, R.; Stratmann, R. E.; Yazyev, O.; Austin, A. J.; Cammi, R.; Pomelli, C.; Ochterski, J. W.; Ayala, P. Y.; Morokuma, K.; Voth, G. A.; Salvador, P.; Dannenberg, J. J.; Zakrzewski, V. G.; Dapprich, S.; Daniels, A. D.; Strain, M. C.; Farkas, O.; Malick, D. K.; Rabuck, A. D.; Raghavachari, K.; Foresman, J. B.; Ortiz, J. V.; Cui, Q.; Baboul, A. G.; Clifford, S.; Cioslowski, J.; Stefanov, B. B.; Liu, G.; Liashenko, A.; Piskorz, P.; Komaromi, I.; Martin, R. L.; Fox, D. J.; Keith, T.; Al-Laham, M. A.; Peng, C. Y.; Nanayakkara, A.; Challacombe, M.; Gill, P. M. W; Johnson, B.; Chen, W.; Wong, M. W.; Gonzalez, C.; Pople, J. A. *Gaussian 03*, revision C.02; Gaussian, Inc.: Wallingford, CT, 2004.
(46) Lindhal, E.; Hess, B.; Van der Spoel, D. *J. Mol. Model.* **2001**, *7*, 306–317.

JM800733H